NANO LETTERS

Letter

pubs.acs.org/NanoLett

Reaching the Theoretical Resonance Quality Factor Limit in Coaxial Plasmonic Nanoresonators Fabricated by Helium Ion Lithography

M. Melli,*[,†,§] A. Polyakov,[†,§] D. Gargas,[†] C. Huynh,[‡] L. Scipioni,[‡] W. Bao,[†] D. F. Ogletree,[†] P. J. Schuck,[†] S. Cabrini,[†] and A. Weber-Bargioni*[,†]

[†]Molecular Foundry, Lawrence Berkeley National Laboratory, Berkeley, California 94720, United States

[‡]Carl Zeiss Microscopy LLC, Peabody, Massachusetts 01960, United States

Supporting Information

ABSTRACT: Optical antenna structures have revolutionized the field of nano-optics by confining light to deep subwavelength dimensions for spectroscopy and sensing. In this work, we fabricated coaxial optical antennae with sub-10-nanometer critical dimensions using helium ion lithography (HIL). Wavelength dependent transmission measurements were used to determine the wavelength-dependent optical response. The quality factor of 11 achieved with our HIL fabricated structures matched the theoretically predicted quality factor for the idealized flawless gold resonators calculated by finite-difference time-domain (FDTD). For comparison, coaxial antennae with 30 nm critical dimensions were fabricated using both HIL and the more common Ga focus ion beam lithography (Ga-FIB). The quality factor of the Ga-FIB resonators was 60% of the ideal HIL results for the same design geometry due to limitations in the Ga-FIB fabrication process.

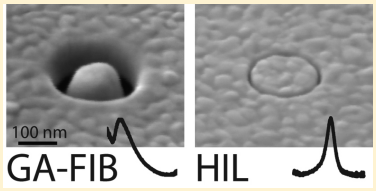

KEYWORDS: *Focus ion beam, helium ion microscope, coaxial apertures, plasmonics, nanofabrication*

Many scientific innovations are experimentally realized years after the theoretical framework has been established since they had to await enabling technologic advances. Nano-optics is a prominent example of that. In 1928, Synge wrote a letter to Einstein proposing to employ the field scattered by a "tiny" metal particle as source for near-field optical imaging.[1] Only recently have advances in nanofabrication enabled the experimental realization of this concept, paving the way to nano- and near-field optics.[2−13] Typically, a gold or silver metal nanostructure is excited by a propagating electromagnetic wave driving the conduction electrons within the metal to collectively oscillate as a surface plasmon polariton (SPP) wave.[14,15] This effect has been used to create optical antennae structures active in the visible spectrum that confine light to deep subwavelength dimensions while enhancing the electromagnetic fields enormously.[16] Applications range from nanospectroscopic imaging[17−23] to novel biosensors with the goal of label-free single molecular sensitivity to plasmonic circuits.

The quality factor of the resonant spectral response of a plasmonic antenna structure, defined as the wavelength of the peak response amplitude divided by the full width at half-maximum, is a figure of merit for design and performance. The electric field enhancement on resonance, the ratio of the electrical field intensity in the antenna gap to the far-field intensity incident on the antenna, is proportional to the quality factor. The resonance and the spectral response of an antenna is a function of its size, shape, and the surrounding environment. The resonator quality factor generally increases as critical dimensions, such as the gap in a bowtie antenna decrease. Hence, much of the work has been dedicated to reproducibly fabricate optical nanoresonators to both spatially and spectrally control light with nanometer precision[24] using state of the art fabrication techniques such as focused ion beam (FIB) milling,[25] electron beam (e-beam) lithography,[26] and induced deposition mask lithography.[27] Resonator critical dimensions are limited by fabrication resolution to >10 nm. In the optical regime and the quasi-static limit, the *Q*-factor reaches a theoretical value of up to 20 for an Au nanoantenna[28] but typically achieves a value of 2 for cavities on the scale of 100 nm and approaches 10 for ultrasmall mode volume nanoresonators.[29] At the dimensions in which the quasi-static approximation is not valid, the shape and the geometry of a nanoresonator strongly influence its optical performance.[30−32] Geometrical deviations from the ideal geometry, such as tapering, sidewall roughness, and corner rounding on length scales comparable to the SPP skin depth, as well as material issues, metal grain structure, effects of adhesion layers, are the reasons for the shortcomings of actual optical antennae compared to their theoretical model structure. In this work, we demonstrate that it is possible to fabricate coaxial optical antennae that match the theoretically predicted resonance quality factor for flawless structures using helium ion lithography (HIL).

The coax antennae represents a metal−insulator−metal waveguide wrapped around itself into a coaxial geometry.[33] When illuminated at resonance, the incident light couples to the SPP, which propagates through the coaxial structure to the other side, where it couples back into the far field. For gap sizes

Received: March 6, 2013
Revised: April 17, 2013
Published: April 25, 2013

   dx.doi.org/10.1021/nl400844a | *Nano Lett.* 2013, 13, 2687−2691

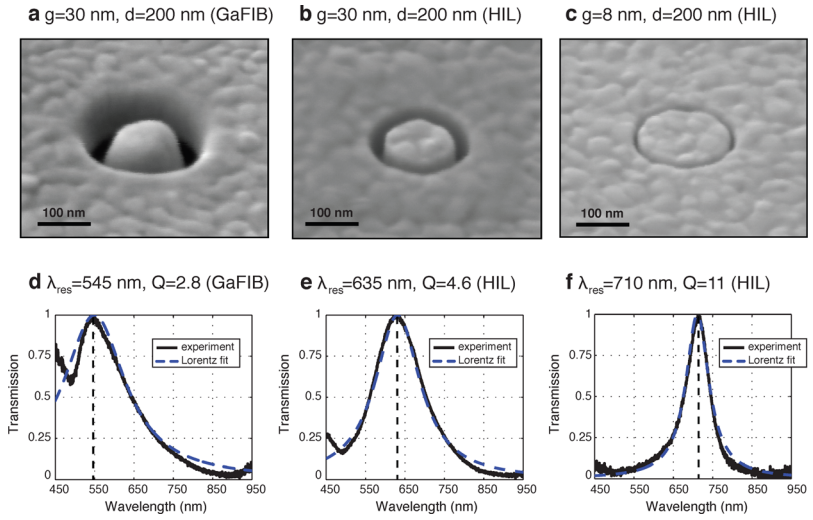

Figure 1. (a–c) SEM images of coaxial apertures with 200 nm diameter in a 100 nm thick gold film. (a) Coax made with Ga-FIB with a nominal gap if 30 nm. (b) Coax made with HIL with a nominal gap if 30 nm. (c) Coax made HIL with a nominal gap if 8 nm. (d–f) Corresponding transmission spectra.

of 20 nm and below, the coaxial aperture becomes a very efficient low-loss plasmonic waveguide[34] and can be employed to create metamaterials[35] where coupled coaxial waveguides are predicted to show a negative effective refractive index in the visible range[36] or for near-field microscopy due to the strong field enhancement and the near field's spatial confinement.[37] Recently, coaxial optical antennae have been also proposed to optically trap nanosized particles,[38] taking advantage of the small mode volume and strong field enhancements to probe nonlinear optical properties.

The resonance wavelength of a coax antenna is determined by the material, the thickness, the diameter of the central pin, and the gap size.[39,40] Coaxial waveguides are typically fabricated using Ga-FIB milling with gap widths, which is the critical dimension, of >20 nm. The resolution is determined by several factors, mostly, the ion beam size, the current, and the ion-substrate interaction. The resolution is also limited by the redeposition of sputtered material, which results in tapered lateral walls. Even if the Ga-FIB's beam waist is in the range of 5 nm, the milled features are greater than 10 nm. This is mainly due to the tails of the Gaussian shaped ion beam, which are low intensity but cover a wide area. In small-diameter annular apertures, used in the coax antennae, this effect is accentuated since the inner pin is constantly exposed to the tails of the beam. All these contributions result in gap sizes larger than 20 nm, a tapered opening to the coax antenna and nonparallel faces of the plasmonic resonator structure which reduce the reflectivity at the end facets of the cavity resulting in a lower *Q*-factor.[37,41] Alternatively, a novel technique based on atomic layer deposition (ALD) can be exploited to fabricate sub-10 nm aperture[42] but exhibits poor control over the wall roughness, affecting the *Q*-factor again. An enormous advance in the fabrication resolution of optical antennae has been recently achieved using the high-resolution helium ion microscopy[43] as a FIB[44,45] to mill features of 5 nm and below. He-FIB, known also as helium ion lithography, enables the reliable production of metallic nanoresonators with impressive fabrication resolution, where deviations from the ideal structure are smaller than the plasmon skin depth.

For this study, coaxial antennae were fabricated in a 100 nm thick Au film using both a state of the art Zeiss XB 1850 Ga-FIB and a Zeiss Orion He ion microscope used in HIL. The substrate was prepared by evaporating a 3 nm thick adhesion layer of Ti on a fused silica coverslip, followed by 100 nm of Au using a semicore e-beam pulsed vapor deposition system. To compare the fabrication dependent spectral response of the antennae and to explore the spectral antenna response for well-defined sub-10 nm gap features three sets of coax antennae were prepared with fixed heights of 100 nm: (1) fixed gap size of 30 nm and varying outer coaxial diameter from 100 to 200 nm, fabricated by a Ga-FIB; (2) same nominal dimensions of 30 nm gap size and varying diameter prepared using HIL; and (3) 8 nm gap size coaxes combined with the equivalent outer diameter variation as in (1) and (2), only possible with HIL. The optical response of the coax apertures was characterized by dark-field spectroscopy (prior to the scanning electron microscopy (SEM) analysis to avoid carbon contamination), where the sample was back illuminated by a 0.8–0.9 numerical aperture (NA) dark-field condenser, and the transmitted light collected by a 60×, 0.7 NA objective lens and routed to a 0.3-m spectrograph (PI Acton) equipped with a LN-cooled CCD camera (Princeton Instruments) for spectral analysis. The transmission spectrum was normalized by measuring the source spectral intensity through a 30 × 30 μm square aperture in the Au film. A background signal, determined by recording the transmission through the undisturbed Au film in the vicinity of the coax, was subtracted from the transmission spectra (additional information about the optical setup can be found in the Supporting Information, Figure S1–S2). The optical response of the coax was then compared to the theoretical response for the ideal geometries, determined by numerical finite difference time domain (FDTD) simulations using the Lumerical software package.[46]

Figure 1 illustrates the fabrication resolution enhancement of HIL (Figure 1b) versus Ga-FIB (Figure 1a), where the profiles of two coaxes with the same nominal dimensions of a 30 nm gap and 200 nm outer diameter are compared. The middle pin of the Ga-FIB coax antenna is deformed by substantially tapering toward the top of the coax and rounding the edges more than 15 nm. In contrast, the HIL coax pin resembles a perfect flat mesa with no apparent damage to the top surface, a parallel gap throughout the antennae and corners with a radius

dx.doi.org/10.1021/nl400844a | *Nano Lett.* 2013, 13, 2687–2691

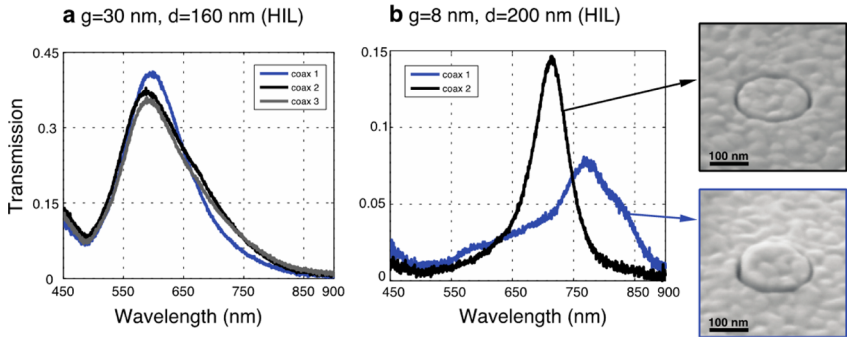

Figure 2. (a) Transmission spectra of three distinct coaxial with the same diameter and a gap of 30 nm. The response is always reproducible. (b) Transmission spectra for 8 nm gap coax. In addition to sharp peak, also broaden and multipeak curves are observed. On the right, SEM images of the corresponding apertures. The size of grain boundaries of the gold of the substrate is comparable with the width of the gap.

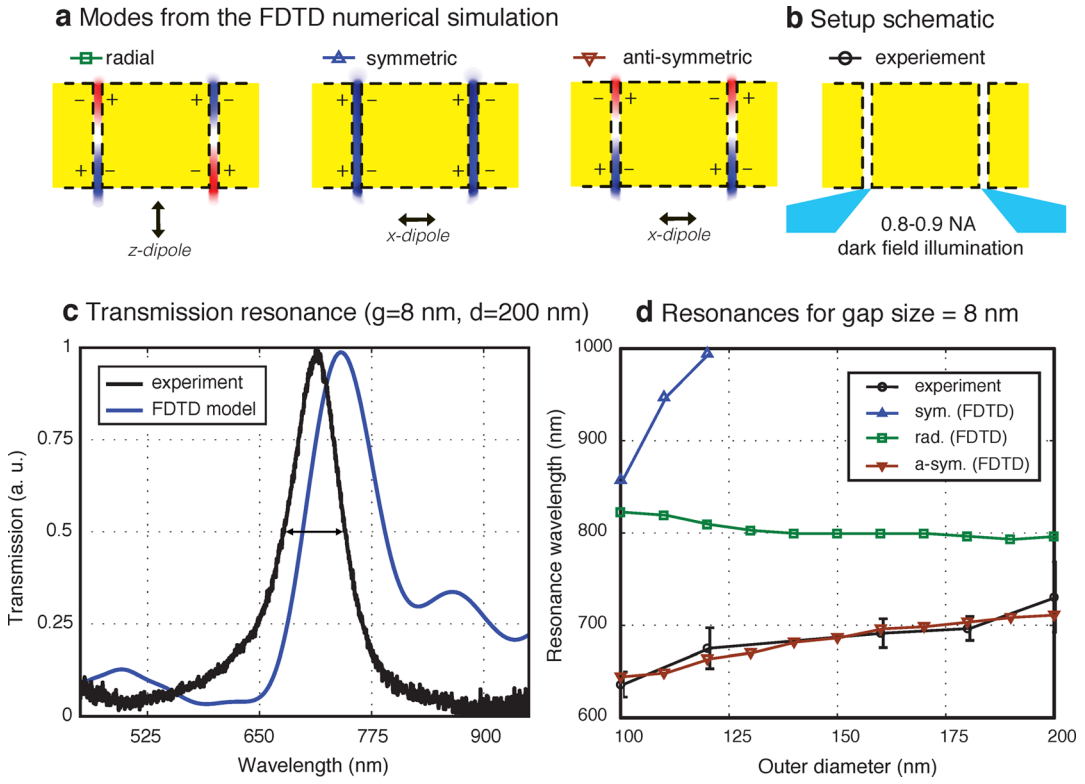

Figure 3. Simulation Results. (a) Field distribution of the first modes from the FDTD simulation. (b) Sketch of the dark-field illumination used in the experiment. (c) Comparison between the experimentally obtained optical transmission signal for d = 200 nm and g = 8 nm coax and the theoretical simulation for the equivalent coax with a perfectly square profile. The small wiggle around 880 nm in the FDTD simulation is due to the long tail of the NIR mode excited by the x-dipole, which is absent from the experimental results due to the dark-field illumination setup. (d) Resonance of the first three modes versus the diameter. The experimental values match the second mode.

sharper then the SEM resolution (<4 nm). The lower interaction volume of the He-ion beam with the sample surface produce much smaller features allowing the reproducible fabrication of coax antennae with 8 nm gaps as shown in Figure 1c. The profile of the coax exhibits the same minimal edge rounding, straight vertical walls, and an unperturbed top surface (see Supporting Information, Figure S3). With the HIL's sub-10 nm gap sizes and defect features smaller than 4 nm, the quality of the substrate material (e.g., grain size) is now the limiting factor for the nano structure's final morphology rather than the fabrication process.

De Waele et al.[41] and Heshmat et al.[34] predicted that parallel sidewalls, minimal sidewall roughness, sharp edges, and minimum gap size are essential in the coax geometry to maximize the coupling efficiency and the resonator's cavity Q-factor. Here we measure the wave dependent resonant optical transmission[47,48] to correlate the optical response of the coaxial resonators with the fabrication dependent morphology (Supporting Information, Figure S4–S5). Light strikes the metal film with the incorporated coaxial antennae from one side and the antennae-mediated transmission is recorded on the opposing side. The incident light is converted into an SPP, which efficiently travels through the coaxial waveguide and is out-coupled on the opposite side as transmitted radiation. For wavelengths at resonance with the coaxial antennae, the SPP will form a standing wave provided the end-facets are sufficiently reflective, which will increase the transmission. Hence, the wavelength dependent transmission is a direct

dx.doi.org/10.1021/nl400844a | Nano Lett. 2013, 13, 2687–2691

measure of the antennae's optical response. Figure 1d−f shows the transmission signal for the various antennae fabricated with Ga-FIB and HIL. The *Q*-factor was determined by fitting the transmission peaks with a Lorentz function. For Ga-FIB fabricated coaxes, the *Q*-factor reached 2.8 and for the equivalent coax fabricated via HIL a much higher *Q*-factor of 4.6 was measured. To clearly show that we are not operating in the quasi-static limit where the *Q*-factor is geometry independent, we compared the *Q*-factors of the HIL fabricated coax to the Ga-FIB fabricated one with the same resonance wavelength but with a different outer diameter (see Supporting Information,Figure S6) showing the same 2 times increase in the *Q*-factor. Therefore the higher *Q*-factor for the HIL structures is due to the improvement of the fabrication resolution, most likely due to the parallel side walls and sharp corner edges at the aperture opening that yield a higher end-facet reflectance. By reducing the last parameter, the gap size, to 8 nm (Figure 1f) the *Q*-factor can be further increased to 11. As the gap size is reduced the plasmon wavelength becomes shorter[49] enhancing the contribution of the retardation effect to improve the *Q*-factor.[50]

The consistency of HIL fabrication is also reflected in the reproducibility of the antennae's optical response. The reproducibility has been tested for various diameters. For each diameter and gap, nine equivalent antennae were fabricated and characterized by transmission measurements. For a series of antennae fabricated to the same specification with a 30 nm gap, the resonance peak, intensity, and shape are almost perfectly reproduced as shown in Figure 2a. For clarity, the raw data of only three antennae are shown (the three representing the full range of variation). For coax antennae with the gap size below 10 nm, the optical response for a few antennae showed a broadened peak as seen as in Figure 2b. Subsequent SEM examination revealed that this broadening was not due to fabrication problems quality but is rather a reflection on the quality of the substrate. Once the gap size and edge sharpness is comparable to the metal grain size, any inhomogeneity larger than the fabricated feature size can have a detrimental effect on the optical response. In this way, the crystalline quality of the metal film becomes the performance bottleneck. To reliably produce antennae with a sub-10 nm feature size for consistent light manipulation both spatially and spectrally requires single crystalline substrates[51] in combination with HIL fabrication.

In this work, we took a full advantage of the HIL's fabrication resolution to achieve parallel side walls, sub-10 nm gaps and small radius of the curvature <4 nm, which is below the plasmon skin depth (~10−20 nm) rendering the structure perfectly square to a propagating SPP wave. We will now show that the optical antennae fabricated with this precision match the theoretical values of an idealized structure. Full size 3D FDTD simulations were performed for ideal coax structures with gap sizes and outer radii corresponding to the dimensions used in the experiment. Mimicking the excitation source used in the dark field spectroscopy was computationally prohibitive, and instead, the different modes of the structure were probed by placing either an *x*- or *z*-polarized dipole source 100 nm below the antenna. Three resonance modes were observed, each excited by a distinct component of the incident radiation. The calculated mode profiles are shown in Figure 3a: the radial mode excited by a *z*-dipole representing a radially polarized source; and the two modes excited by the *x*-dipole, the symmetric mode, excited by the normal-incidence component, and the antisymmetric mode, excited by the components with a high angles of incidence, which best approximates the experimental arrangement (Figure 3b, full simulation details are provided in the Supporting Information, Figure S7−S10). Figure 3c shows the direct comparison between the experimentally obtained transmission signal for d = 200 nm and g = 8 nm coax and the theoretical simulation for the equivalent coax with a perfect square profile. Both the computed resonance wavelength and *Q*-factor agree well with the experimental data exhibiting only a minor resonance peak shift that is attributed to small variation in the value of the gold film thickness (see Supporting Information, Figure S10). Most notably the *Q*-factor obtained in the simulation of a perfect coax structure is 9, close to the best-case experimental value of 11. The tails of the NIR transmission peak, which is absent in the experiment, causes the transmission peak broadening resulting in a slightly lower *Q*-factor from the simulation. The overall agreement of the experimentally achieved value with theory is further evidence that the HIL fabricated antennae are performing spectrally at the limit of an ideal plasmonic antenna.

In dark-field illumination, only the antisymmetric mode was excited, however, in the FDTD calculations using the *x*-dipole source, both the symmetric and the antisymmetric modes were observed, with the former dominating the spectral response for the coax outer diameter below 150 nm. Therefore, a near-field analysis was used to calculate the resonance position of the antisymmetric mode, as shown in Figure 3d. A good agreement between the measured resonance and the FDTD model is seen for the entire set of the HIL-fabricated structures. In each case, the *Q*-factor was measured to be 10 on average experimentally and 9 from the FDTD simulation demonstrating the consistency in fabricating optimum quality resonance antennae using HIL.

In summary, we have shown that the optical performance of HIL-fabricated metallic nanoresonators matches that calculated for ideal structures. We have demonstrated a dramatic improvement in the optical response between the HIL and Ga-FIB fabricated-coaxial structures and have shown that for a coaxial antenna with a gap of 8 nm the resonance quality factor of 11 corresponds to the theoretical predicted optical response of an ideal coaxial structure. The remaining factor limiting fabrication is the quality (crystallinity) of the substrate metal, which hampers reproducibility. Since we experimentally reached the maximum resonator quality factor for an Au dipolar optical antenna, an improvement in the fabrication resolution should only increase the spatial field confinement and therefore field enhancement. It would be interesting to measure the *Q*-factor for smaller gap structures fabricated in single crystal metal films. The reproducible, high-resolution fabrication capabilities of the He ion microscope operated as an HIL will have an enormous impact on the development of plasmonic circuits, spatial manipulation of light on the single digit nanometer scale, prototyping of label-free optical antenna-based sensors, and especially incorporating optical antennae on scanning probe tips for reliable high performance near-field optical microscopy and spectroscopy.

■ ASSOCIATED CONTENT

Supporting Information

Additional information and figures. This material is available free of charge via the Internet at http://pubs.acs.org.

AUTHOR INFORMATION

Corresponding Author

*E-mail: (M.M.)mmelli@lbl.gov; (A.W.-B.)afweber-bargioni@lbl.gov.

Author Contributions

§M.M. and A.P. contributed equally to this work.

Notes

The authors declare no competing financial interest.

ACKNOWLEDGMENTS

The authors thank our colleagues at the Molecular Foundry for stimulating discussion, advice, and assistance, in particular Edward Barnard. A.P. thanks H. A. Padmore for providing the computational resources for the numerical simulation. Work at the Molecular Foundry was supported by the U.S. Department of Energy (DOE), Office of Basic Energy Sciences, Scientific User Facilities Division, under contract no. DE-AC02-05CH11231.

REFERENCES

(1) Novotny, L. *Phys. Today* **2011**, *64* (7), 47.
(2) Zayats, A. V.; Smolyaninov, I. I.; Maradudin, A. A. *Phys. Rep.*. **2005**, *408* (3−4), 131−314.
(3) Fischer, H.; Martin, O. J. F. *Opt. Express* **2008**, *16* (12), 9144−9154.
(4) Ghenuche, P.; Cherukulappurath, S.; Quidant, R. *New J. Phys.* **2008**, 10.
(5) Novotny, L. *Phys. Rev. Lett.* **2007**, *98*, 26.
(6) Schuck, P. J.; Fromm, D. P.; Sundaramurthy, A.; Kino, G. S.; Moerner, W. E. *Phys. Rev. Lett.* **2005**, *94*, 1.
(7) Kelly, K. L.; Coronado, E.; Zhao, L. L.; Schatz, G. C. *J. Phys. Chem. B* **2003**, *107* (3), 668−677.
(8) Lal, S.; Link, S.; Halas, N. J. *Nat. Photonics* **2007**, *1* (11), 641−648.
(9) Muhlschlegel, P.; Eisler, H. J.; Martin, O. J. F.; Hecht, B.; Pohl, D. W. *Science* **2005**, *308* (5728), 1607−1609.
(10) Hrelescu, C.; Sau, T. K.; Rogach, A. L.; Jackel, F.; Feldmann, J. *Appl. Phys. Lett.* **2009**, *94*, 15.
(11) Hicks, E. M.; Zou, S. L.; Schatz, G. C.; Spears, K. G.; Van Duyne, R. P.; Gunnarsson, L.; Rindzevicius, T.; Kasemo, B.; Kall, M. *Nano Lett.* **2005**, *5* (6), 1065−1070.
(12) Biagioni, P.; Huang, J. S.; Duo, L.; Finazzi, M.; Hecht, B. *Phys. Rev. Lett.* **2009**, *102*, 25.
(13) Taminiau, T. H.; Moerland, R. J.; Segerink, F. B.; Kuipers, L.; van Hulst, N. F. *Nano Lett.* **2007**, *7* (1), 28−33.
(14) Boardman, A.; Brongersma, M.; Stockman, M.; Wegener, M. *J. Opt. Soc. Am. B* **2009**, *26*, 12.
(15) Maier, S. A.; Atwater, H. A. *J. Appl. Phys.* **2005**, *98* (1), 011101.
(16) Polyakov, A.; Senft, C.; Thompson, K. F.; Feng, J.; Cabrini, S.; Schuck, P. J.; Padmore, H. A.; Peppernick, S. J.; Hess, W. P. *Phys. Rev. Lett.* **2013**, *110* (7), 076802.
(17) De Angelis, F.; Das, G.; Candeloro, P.; Patrini, M.; Galli, M.; Bek, A.; Lazzarino, M.; Maksymov, I.; Liberale, C.; Andreani, L. C.; Di Fabrizio, E. *Nat. Nanotechnol.* **2010**, *5* (1), 67−72.
(18) Fleischer, M.; Stanciu, C.; Stade, F.; Stadler, J.; Braun, K.; Heeren, A.; Haeffner, M.; Kern, D. P.; Meixner, A. J. *Appl. Phys. Lett.* **2008**, *93*, 11.
(19) Gerton, J. M.; Wade, L. A.; Lessard, G. A.; Ma, Z.; Quake, S. R. *Phys. Rev. Lett.* **2004**, *93*, 18.
(20) Kalkbrenner, T.; Ramstein, M.; Mlynek, J.; Sandoghdar, V. *J. Microsc. (Oxford, U.K.)* **2001**, *202*, 72−76.
(21) Berweger, S.; Atkin, J. M.; Xu, X. G.; Olmon, R. L.; Raschke, M. B. *Nano Lett.* **2011**, *11* (10), 4309−4313.
(22) Kosako, T.; Kadoya, Y.; Hofmann, H. F. *Nat. Photonics* **2010**, *4* (5), 312−315.
(23) Bao, W.; Melli, M.; Caselli, N.; Riboli, F.; Wiersma, D. S.; Staffaroni, M.; Choo, H.; Ogletree, D. F.; Aloni, S.; Bokor, J.; Cabrini, S.; Intonti, F.; Salmeron, M. B.; Yablonovitch, E.; Schuck, P. J.; Weber-Bargioni, A. *Science* **2012**, *338* (6112), 1317−1321.
(24) McLeod, A.; Weber-Bargioni, A.; Zhang, Z.; Dhuey, S.; Harteneck, B.; Neaton, J. B.; Cabrini, S.; Schuck, P. J. *Phys. Rev. Lett.* **2011**, *106* (3), 037402.
(25) Farahani, J. N.; Pohl, D. W.; Eisler, H. J.; Hecht, B. *Phys. Rev. Lett.* **2005**, *95*, 1.
(26) Wissert, M. D.; Schell, A. W.; Ilin, K. S.; Siegel, M.; Eisler, H. J. *Nanotechnology* **2009**, *20*, 42.
(27) Fleischer, M.; Weber-Bargioni, A.; Cabrini, S.; Kern, D. P. *Microelectron. Eng.* **2011**, *88* (8), 2247−2250.
(28) Wang, F.; Shen, Y. R. *Phys. Rev. Lett.* **2006**, *97* (20), 206806.
(29) Ni, C. Y. A.; Shu-Wei, C.; Shun Lien, C.; Schuck, P. J. *J. Lightwave Technol.* **2011**, *29* (20), 3107−3114.
(30) Vesseur, E. J. R.; García de Abajo, F. J.; Polman, A. *Nano Lett.* **2009**, *9* (9), 3147−3150.
(31) Yang, S.-C.; Kobori, H.; He, C.-L.; Lin, M.-H.; Chen, H.-Y.; Li, C.; Kanehara, M.; Teranishi, T.; Gwo, S. *Nano Lett.* **2010**, *10* (2), 632−637.
(32) Kern, J.; Großmann, S.; Tarakina, N. V.; Häckel, T.; Emmerling, M.; Kamp, M.; Huang, J.-S.; Biagioni, P.; Prangsma, J. C.; Hecht, B. *Nano Lett.* **2012**, *12* (11), 5504−5509.
(33) Baida, F.; Belkhir, A.; Van Labeke, D.; Lamrous, O. *Phys. Rev. B* **2006**, *74*, 20.
(34) Heshmat, B.; Li, D.; Darcie, T. E.; Gordon, R. *Opt. Express* **2011**, *19* (7), 5912−5923.
(35) de Waele, R.; Burgos, S. P.; Atwater, H. A.; Polman, A. *Opt. Express* **2010**, *18* (12), 12770−12778.
(36) Burgos, S. P.; de Waele, R.; Polman, A.; Atwater, H. A. *Nat. Mater.* **2010**, *9* (5), 407−412.
(37) Weber-Bargioni, A.; Schwartzberg, A.; Cornaglia, M.; Ismach, A.; Urban, J. J.; Pang, Y.; Gordon, R.; Bokor, J.; Salmeron, M. B.; Ogletree, D. F.; Ashby, P.; Cabrini, S.; Schuck, P. J. *Nano Lett.* **2011**, *11* (3), 1201−1207.
(38) Saleh, A. A. E.; Dionne, J. A. *Nano Lett.* **2012**, *12* (11), 5581−5586.
(39) Li, D.; Gordon, R. *Phys. Rev. A* **2010**, *82*, 4.
(40) Catrysse, P. B.; Fan, S. *Appl. Phys. Lett.* **2009**, *94*, 23.
(41) de Waele, R.; Burgos, S. P.; Polman, A.; Atwater, H. A. *Nano Lett.* **2009**, *9* (8), 2832−2837.
(42) Im, H.; Bantz, K. C.; Lindquist, N. C.; Haynes, C. L.; Oh, S.-H. *Nano Lett.* **2010**, *10* (6), 2231−2236.
(43) Hill, R.; Notte, J. A.; Scipioni, L.; Hawkes, P. W. Scanning Helium Ion Microscopy. *Advances in Imaging and Electron Physics*; Academic Press: New York, 2012; pp 65−148.
(44) Scipioni, L.; Ferranti, D. C.; Smentkowski, V. S.; Potyrailo, R. A. *J. Vac. Sci. Technol. B* **2010**, *28* (6), C6P18−C6P23.
(45) Bell, D. C.; Lemme, M. C.; Stern, L. A.; Williams, J. R.; Marcus, C. M. *Nanotechnology* **2009**, *20* (45), 455301.
(46) Lumerical Solutions, www.lumerical.com (accessed 2013).
(47) Ebbesen, T. W.; Lezec, H. J.; Ghaemi, H. F.; Thio, T.; Wolff, P. A. *Nature* **1998**, *391* (6668), 667−669.
(48) Orbons, S. M.; Roberts, A.; Jamieson, D. N.; Haftel, M. I.; Schlockermann, C.; Freeman, D.; Luther-Davies, B. *Appl. Phys. Lett.* **2007**, *90* (25), 251107.
(49) Miyazaki, H.; Kurokawa, Y. *Phys. Rev. Lett.* **2006**, *96*, 9.
(50) Feigenbaum, E.; Orenstein, M. *Phys. Rev. Lett.* **2008**, *101*, 16.
(51) Huang, J.-S.; Callegari, V.; Geisler, P.; Brüning, C.; Kern, J.; Prangsma, J. C.; Wu, X.; Feichtner, T.; Ziegler, J.; Weinmann, P.; Kamp, M.; Forchel, A.; Biagioni, P.; Sennhauser, U.; Hecht, B. *Nat. Commun.* **2010**, *1*, 150.

NOTE ADDED AFTER ASAP PUBLICATION

Figures 1 and 3 have been updated in the version published ASAP on May 1, 2013. The revised version was re-posted on May 14, 2013.